NANO LETTERS
Letter
Cite This: Nano Lett. 2018, 18, 1564−1574
pubs.acs.org/NanoLett

Magneto-Spin−Orbit Graphene: Interplay between Exchange and Spin−Orbit Couplings

Artem G. Rybkin,[*,†] Anna A. Rybkina,[‡] Mikhail M. Otrokov,[§,∥,‡,⊥] Oleg Yu. Vilkov,[‡] Ilya I. Klimovskikh,[‡] Anatoly E. Petukhov,[‡] Maria V. Filianina,[‡] Vladimir Yu. Voroshnin,[‡] Igor P. Rusinov,[∥,‡] Arthur Ernst,[#,∇] Andrés Arnau,[§,⊥] Evgueni V. Chulkov,[‡,§,⊥,∥] and Alexander M. Shikin[‡]

[†]Research Park, Saint Petersburg State University, 198504 Saint Petersburg, Russia

[‡]Saint Petersburg State University, 198504 Saint Petersburg, Russia

[§]Donostia International Physics Center (DIPC), Paseo de Manuel Lardizabal 4, 20018 San Sebastián/Donostia, Spain

[∥]Tomsk State University, 634050 Tomsk, Russia

[⊥]Departamento de Física de Materiales UPV/EHU, Centro de Física de Materiales CFM - MPC and Centro Mixto CSIC-UPV/EHU, 20080 San Sebastián/Donostia, Spain

[#]Max-Planck-Institut für Mikrostrukturphysik, Weinberg 2, D-06120 Halle, Germany

[∇]Institut für Theoretische Physik, Johannes Kepler Universität, A 4040 Linz, Austria

Supporting Information

ABSTRACT: A rich class of spintronics-relevant phenomena require implementation of robust magnetism and/or strong spin−orbit coupling (SOC) to graphene, but both properties are completely alien to it. Here, we for the first time experimentally demonstrate that a quasi-freestanding character, strong exchange splitting and giant SOC are perfectly achievable in graphene at once. Using angle- and spin-resolved photoemission spectroscopy, we show that the Dirac state in the Au-intercalated graphene on Co(0001) experiences giant splitting (up to 0.2 eV) while being by no means distorted due to interaction with the substrate. Our calculations, based on the density functional theory, reveal the splitting to stem from the combined action of the Co thin film in-plane exchange field and Au-induced Rashba SOC. Scanning tunneling microscopy data suggest that the peculiar reconstruction of the Au/Co(0001) interface is responsible for the exchange field transfer to graphene. The realization of this "magneto-spin−orbit" version of graphene opens new frontiers for both applied and fundamental studies using its unusual electronic bandstructure.

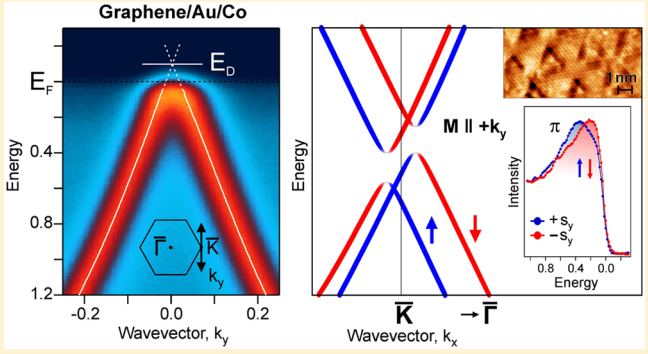

KEYWORDS: *Graphene, spin−orbit and exchange coupling, electronic structure, angle- and spin-resolved photoemission spectroscopy, scanning tunneling microscopy, ab initio calculations*

Extending graphene's functionalities beyond those intrinsically inherent to it has become a great challenge of contemporary solid state physics, materials science, and nanotechnology.[1−6] In particular, being a nonmagnetic material with a weak spin−orbit coupling (SOC), graphene inspires a great quest for the ways of modifying these properties, thus offering prospects for the appearance of exotic phenomena and novel applications. For example, the enhancement of SOC in graphene would enable the efficient generation of pure spin currents based on the spin Hall effect,[6] as has already been observed.[7] It could also facilitate the eventual realization of its quantized version in the carbon honeycomb lattice.[8] A multitude of effects have also been predicted to appear in graphene when it is magnetized in a controlled manner, for example, the gate tunable exchange bias,[9] spin-transfer torque,[6,10] magnetoresistance and spin filtering,[2,5,11] just to name a few. Actually, a combination of strong SOC and robust magnetism could provide a playground for the observation of the quantum anomalous Hall effect,[12] spin−orbit torque,[13] and other phenomena,[14,15] thus boosting the already established high application potential of graphene to an unprecedented limit. However, great care should be taken when modifying its properties in order to preserve the intrinsic characteristics of graphene that make it so attractive, namely, a linear dispersion of the electronic bands close to the Fermi level and ultrahigh carrier mobility.[5,16−23]

So far, several approaches to enhance spin−orbit effects in graphene have been proposed. The hydrogenation[7] or fluorination[22] of graphene as well as proximity of heavy compound[21,24]

Received: April 12, 2017
Revised: January 18, 2018
Published: January 24, 2018

DOI: 10.1021/acs.nanolett.7b01548
Nano Lett. 2018, 18, 1564−1574

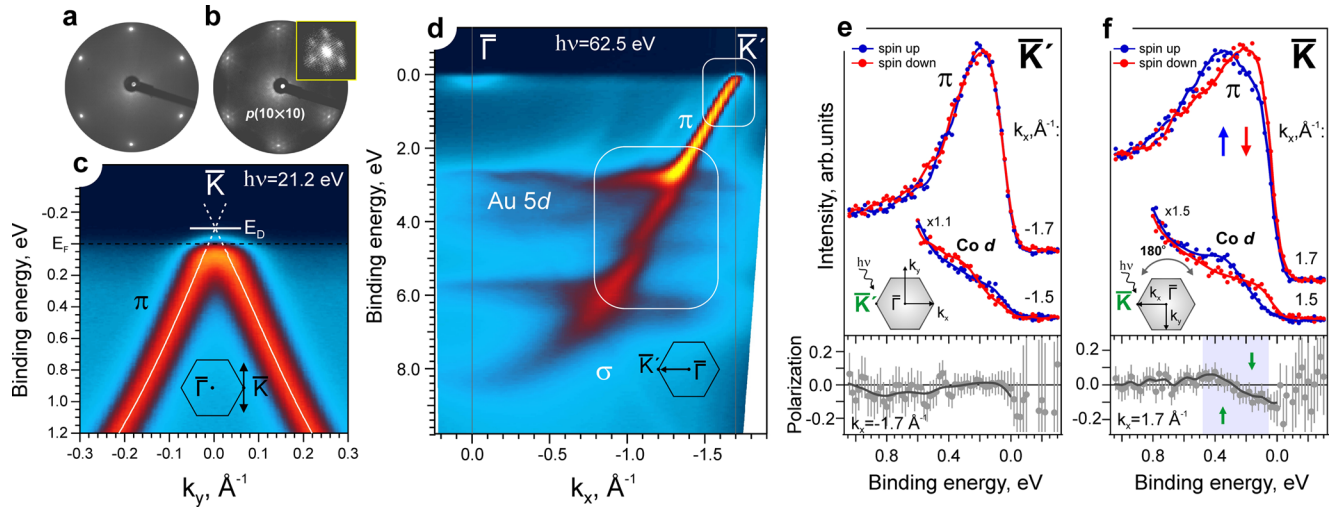

Figure 1. LEED and ARPES insights into the crystal, electronic, and spin structures of graphene/Co before and after Au intercalation. (a,b) LEED patterns of graphene/Co(0001) and graphene/Au/Co(0001), respectively, obtained with an electron beam energy of 113 eV. The inset in (b) shows a zoom of a (1×1) spot with its six satellites. (c) Dispersion of the graphene/Au/Co(0001) Dirac π-state near the $\bar{K}$ point of the 2D BZ, measured along the k_y direction using a photon energy of 21.2 eV (solid white lines show the result of momentum distribution curves fitting with two Lorentzian peak functions). (d) ARPES data of graphene/Au/Co(0001) acquired in the $\bar{\Gamma}\bar{K}'$ direction of the 2D BZ with a photon energy of 62.5 eV. (e,f) Photoemission spectra with angle and spin resolution measured in the $\bar{K}'$ and $\bar{K}$ points valleys, respectively ($h\nu$ = 62.5 eV). The panels below the spin-resolved spectra display the measured spin polarizations. The data taken at $k_{\parallel} = 1.7$ Å^{-1} correspond to the signal coming from the graphene π-band near the Fermi level, while the Co d-states are probed at $k_{\parallel} = 1.5$ Å^{-1} (the graphene- and gold-derived states are lying well below them; we associate the Co d-states in panels e and f with the edges of the spin-polarized d-bands, bordering the local bandgaps, see Supporting Information Note B1). In (e,f), blue and red colors denote opposite sign projections of an electron spin vector, lying in-plane and directed perpendicular to the momentum. The spin-resolved energy distribution curve (EDC) data without smoothing of the polarization function are shown by red and blue points.

are known as the ways to increase its intrinsic SOC. On the other hand, the intercalation of heavy species, for example, Au,[25−27] has been found to yield a giant Rashba effect in graphene.[28,29] Strong enhancement of SOC has also been reported for a partially and fully Pb-intercalated graphene on Ir[30] and Pt(111),[31] respectively, both cases pointing toward the quantum-spin-Hall-like state in the carbon honeycomb. Making graphene magnetic represents another great challenge. The most straightforward way is its synthesis on the magnetic substrates such as Ni(111) and Co(0001).[32−36] However, there is a price to pay: the pristine electronic bandstructure of freestanding graphene is lost due to hybridization of the π-state and underlying metal surface states.[32−36] Another alternative is based on the use of nonmagnetic and relatively inert substrates that allow tuning graphene's magnetization via the creation of isolated vacancies[37−41] or light atoms adsorption.[37,42−44] These methods have proven experimentally feasible, although requiring a precise control of the vacancies/adsorbates distribution, which appears to be quite challenging. Despite all these efforts, presently, a sizable spin splitting originating from the combined action of the SOC and induced magnetization in graphene has not been measured.

Here, we report the first experimental evidence of a quasi-freestanding graphene bandstructure characterized by strongly enhanced exchange and Rashba effects, whereby we call it magneto-spin−orbit graphene. Applying angle- and spin-resolved photoemission spectroscopy to the Au-intercalated graphene on Co(0001)/W(110), we observe a giant spin splitting (up to 200 meV) of the Dirac state whose linear dispersion is nonetheless largely preserved. On the basis of the density functional theory (DFT) calculations, we decisively establish the splitting to stem from the combined action of the Co-film-derived in-plane exchange field and Au-induced Rashba SOC, the hallmark of such a phenomenon being a strong bandstructure asymmetry with respect to the Brillouin zone (BZ) center. Further scanning tunneling microscopy (STM) measurements reveal that the exchange field transfer from the Co film to graphene is facilitated by a peculiar reconstruction at the hidden Au/Co(0001) interface. These results represent a clear achievement of a case in which quasi-freestanding graphene simultaneously shows strong spin−orbit and magnetic effects without external fields, which opens promising avenues for realization of the above-room-temperature graphene spintronics.

Spin Splitting Asymmetry. We start from structural characterization of the graphene/Co(0001)/W(110) before and after the gold intercalation. The low energy electron diffraction (LEED) pattern, obtained for the chemical vapor deposition (CVD)-grown single graphene layer on Co(0001), represents a perfect hexagon of sharp and bright reflexes (Figure 1a). One can conclude that the graphene sheet formed is of high quality and is commensurate with the Co(0001) surface, showing a (1×1) structure, in agreement with ref 45. Under the synthesis conditions used, graphene grows with one sublattice being placed atop the surface layer Co atoms and the other falling in the fcc hollow sites of Co(0001).[46] The bonds between the on-top graphene atoms and the underlying Co ones stabilize the commensurate growth favored by a small mismatch of the lattices. However, despite a chemical bonding between graphene and Co substrate, a gold layer can be intercalated.[35] As can be seen in Figure 1b showing the LEED pattern after the Au intercalation, a fine structure composed of six satellites surrounding each (1×1) spot appears that can be identified as a $p(10 \times 10)$ superstructure. Similar $p(9 \times 9)$ periodicity was previously observed for the gold-intercalated graphene/Ni(111).[25,47]

Another strong indication of the successful intercalation comes from the inspection of the photoemission spectra of the graphene/Co sample before and after exposing it to gold. It is well-known, that the graphene's electronic structure is strongly

DOI: 10.1021/acs.nanolett.7b01548
Nano Lett. 2018, 18, 1564−1574

modified by interaction with ferromagnetic 3d substrates.[35,45,47,48] However, intercalation of a nonmagnetic metal atoms helps to recover graphene's bandstructure close to that of the freestanding one.[25,26,49] Indeed, in stark contrast to the graphene/Co system, the gold-intercalated one is characterized by a nice linearly dispersing π-state up to binding energies (BEs) of 2 eV, the Dirac point (DP) being located at ~100 meV above E_F (Figure 1c,d). Importantly, for a quasi-freestanding graphene low-energy band structure formation the gold d-states are located in the 2−6 eV BE region, where the deviations from the linear dispersion due to spin-dependent avoided-crossing effects[25,26] are seen (marked by a large rounded rectangle in Figure 1d). Next, the absence of the photoemission signal in the second BZ along the $\bar{K}\bar{M}$ $\|k_x$ direction (see Figure 2) indicates that the A−B sublattice

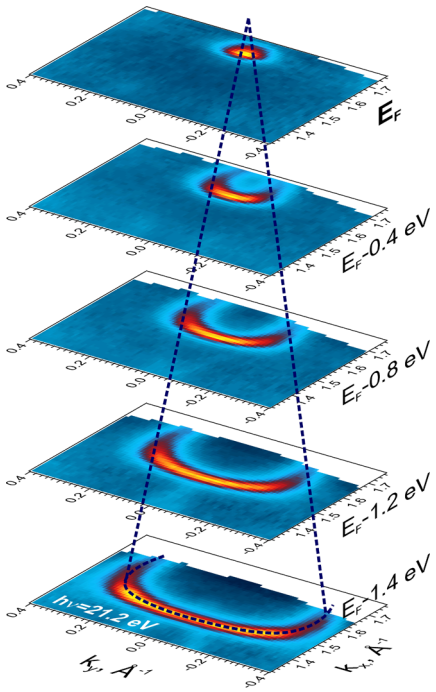

Figure 2. Constant-energy maps of the angle-resolved photoemission intensity for graphene/Au/Co(0001) at the $\bar{K}$ point.

symmetry is no longer broken[50,51] after the gold intercalation, unlike in the graphene/Co case.[45] As further confirmed using STM measurements, a $p(10 \times 10)$ superstructure favors neither the A−B symmetry breaking nor increase of the graphene's intrinsic SOC. Consequently, the DP gap formation can be excluded in our graphene/Au/Co(0001). Thus, the electronic structure of the Au-intercalated graphene on Co(0001) turns out to be largely similar to that of freestanding graphene with its linear dispersion maintained, the Dirac cone being slightly p-doped, and showing no clear signatures of the DP gap opening. However, as we demonstrate below, there is a fundamental difference with respect to the freestanding graphene case: a huge spin splitting of the π-band.

Strong or even giant spin−orbit effects may be expected upon intercalation of an element as heavy as gold below graphene.[25,30,31] To check their presence in graphene/Au/Co(0001), we have performed photoemission measurements with spin resolution. Surprisingly, we first do not find any noticeable splitting of the π-state at the $\bar{K}'$ point (-1.7 Å^{-1}) with the error of 20 meV, as one can see in Figure 1e that displays a spin-resolved spectrum of graphene's Dirac cone. We then have measured a spin-resolved spectrum at the $\bar{K}$ point ($k_\|$ = 1.7 Å^{-1}) and in stark contrast found a giant spin splitting of the π-state with a magnitude up to 150 ± 20 meV, see Figure 1f. It should be noted here that this measurement has been done by rotating the sample by 180° around the normal emission axis (hereafter, azimuth angle rotation), as it is shown in the bottom left corner of the figure. The reason for that is to keep the experiment geometry, that is, the angles of photon incidence and photoelectron emission. The measurement without azimuth angle rotation has also been performed and the result obtained agrees well with that shown in Figure 1e,f, see Note A3 of the Supporting Information. The asymmetry of the spin splitting for the $\pm k_\|$ directions in the 2D BZ implies its mechanism lies beyond simple Rashba model in graphene.

Combination of Rashba SOC and Exchange Field. A common reason for the $\pm k_\|$ asymmetry of the electronic structure is a lifting of the time-reversal symmetry. Because of the magnetic nature of the Co substrate, one may suggest its magnetization to play a role in the formation of the band and spin structure observed. Particularly, such an asymmetry can be brought about by a so-called "Rashba+Exchange" effect that was first seen for the rare-earth metal surfaces,[52] but later has also been discussed in relation to graphene.[33] The effect requires, however, the magnetization vector to lie within the surface plane, while it is well-known that bulk hcp Co has an easy axis along (0001), that is, perpendicular to the basal plane.[53] In contrast, for the thin film system showing the same surface, this axis lies in-plane due to surface anisotropy effects.[54,55] This is exactly what takes place in our Co(0001) film grown on W(110) substrate, for which magnetization is known to be oriented along the W[1$\bar{1}$0] direction in films with thickness of more than 3 and up to at least 50 monolayers.[54,55] Namely, since the thickness of our Co(0001) film (~95 Å or 46 monolayers) is close to the mentioned upper limit, we have checked the easy axis direction with the spin-resolved ARPES measurements. This has been done by probing the Co d-states both near the $\bar{K}$ point (at $k_\|$ = 1.5 Å^{-1} along k_x) and at the $\bar{\Gamma}$ point, using a normal emission mode. In the former case, we find that there is no spin polarization along k_x, while there is along k_y (Figure 1e,f). In the latter case, the measurements with the 120 eV photon energy (Note A4.1 of the Supporting Information) show that the polarization axis is rotated together with the sample, proving our Co(0001) film to be spontaneously magnetized in-plane along the [1$\bar{1}$00] axis (i.e., parallel to $-k_y$).

To confirm that it is a combined action of the gold-induced Rashba SOC and a Co-derived in-plane exchange field that produces such an effect, we have performed spin-resolved photoemission measurements after applying external magnetic field first in the [01$\bar{1}$0] direction and then in the one opposite to it. We begin with checking the normal emission spectra to monitor the Co d-states polarization after the field application. The results of the measurements are shown in Figure 3a,b. Note that the photon energy of 21.2 eV has been chosen for a clear comparison with the data available in literature[55,56] and we indeed find a good agreement. Importantly, by comparing the two spectra shown in Figure 3a,b, one can clearly see the reversal of the Co 3d-states spin polarization indicative of the sample remagnetization.

We then concentrate on the BZ corners to reveal graphene's π-state changes accompanying sample remagnetization. Revisiting the $\bar{K}$ and $\bar{K}'$ points with the 21.2 eV photons after the field application along the $-k_y$ direction (one of the sample's easy magnetization axes), we find a substantially increased spin splitting of 200 ± 40 meV in the $\bar{K}$ point (Figure 3c; c.f. Figure 1f), and a

DOI: 10.1021/acs.nanolett.7b01548
Nano Lett. 2018, 18, 1564−1574

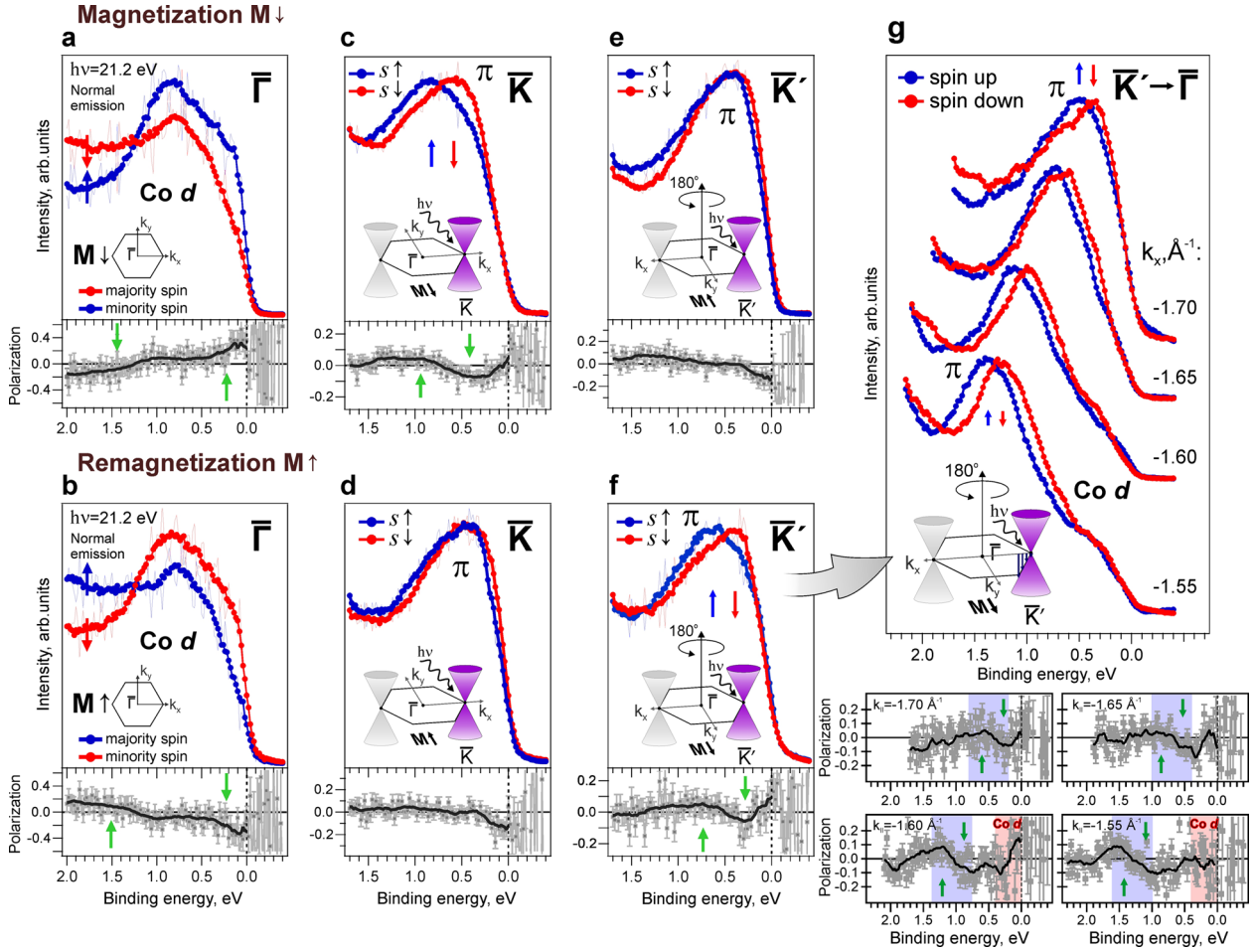

Figure 3. Spin splittings in graphene/Au/Co(0001) after magnetization and remagnetization by external field. (a,b) Spin-resolved normal photoemission spectrum of the Co d-band after the external magnetic field application along the $[01\bar{1}0]$ (magnetization) and $[0\bar{1}10]$ directions (remagnetization), respectively. Color coding is the same as in Figure 1. (c−f) Spin-resolved photoemission spectra of the graphene π-states at the $\bar{K}$ and $\bar{K}'$ points of the 2D BZ after the magnetization (c,e) and remagnetization (d,f). The measurements at $\bar{K}'$ have been done after a 180° azimuth angle rotation of the previously (re)magnetized sample (see text for explanations). The spin-resolved EDC data without smoothing of the polarization function are shown by thin red and blue lines. (g) Spin-resolved photoemission spectra of the graphene π-state taken along the $\bar{K}'\bar{\Gamma}$ direction at several $k_{\|}$ after the remagnetization. The panels below the spin-resolved spectra display the measured spin polarizations. All measurements have been performed with a photon energy of 21.2 eV.

splitting of about 40 ± 40 meV in the $\bar{K}'$ one (Figure 3e; c.f. Figure 1e). To find signatures of such an asymmetry in the spin-integrated photoemission spectrum, we have performed a careful EDC analysis in both the $\bar{K}$ and $\bar{K}'$ valleys. Figure 4 shows the spin-integrated EDCs near the $\bar{K}'$ (panel a, gold color) and $\bar{K}$ points (panel b, green color). The measurements have been performed along the $\bar{\Gamma}\bar{K}$ and $\bar{\Gamma}\bar{K}'$ directions for the magnetization pointing along $+k_y$ ($[0\bar{1}10]$). It is evident from the first glance, that the peaks near $\bar{K}'$ are significantly wider than those near $\bar{K}$ (fwhm's of ∼500−530 and ∼410−450 meV, respectively), which is consistent with the fact that after the sample remagnetization (Figure 3d,f,g) the measured spin splitting in the $\bar{K}'$ valley is much larger than in the $\bar{K}$ one. It should be noted that near the $\bar{K}'$ point, the fwhm decreases abruptly which is due to the Fermi level proximity resulting into π-states cutoff (see the topmost EDC in Figure 4a). The fitting of the second from the top peaks yields two main components (shown in red and blue) that reveal different energy separation between their maxima. These blue and red peaks can be nicely identified as the spin-split states based on the spin-ARPES data shown in Figure 3: the spin splitting near the $\bar{K}'$ point is giant (200 meV, Figure 3f and Figure 4a), while near the $\bar{K}$ point it is much smaller (40−50 meV, Figure 3d and Figure 4b). According to the EDC analysis, the fwhm of each of the two components of the π-state is large, reaching ∼380 meV, that does not allow one to clearly see the spin splitting between them in the spin-integrated ARPES. Finally, it should be noted that based on the $s_x + s_z$ spin polarization data we find the same giant and asymmetric spin splitting of the graphene states, as in the case of the s_y component behavior (Supporting Information Note A6).

It should be noted that after the magnetization (M↓ in Figure 3) the spin splitting near $\bar{K}$ increases significantly as compared to that in Figure 1f, which may be attributed to the growth of the domains that are getting magnetized in the $[01\bar{1}0]$ direction by the field. We note that the spin splitting observed appears to be of a large magnitude for a graphene with preserved linear dispersion relation and retained group velocity. A two times smaller spin splitting has previously been reported for the gold-intercalated graphene/Ni(111)[25] and attributed to the pure Rashba effect. However, in graphene/Au/Co(0001), in agreement with what one can expect assuming the Rashba+Exchange mechanism,[33,52] the band and spin structures change symmetrically relative to the 2D BZ center after

DOI: 10.1021/acs.nanolett.7b01548
Nano Lett. 2018, 18, 1564−1574

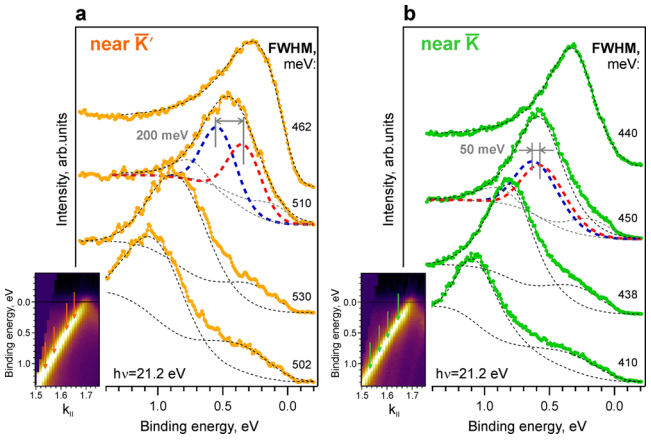

Figure 4. Energy distribution curves near the $\bar{K}$ and $\bar{K}'$ points with 2D data plots of ARPES intensity versus k_x. (a,b) Spin-integrated EDC photoemission spectra of the graphene π-states with fitting of the main peaks and the background at $k_{\parallel} = -1.63$ and 1.61 Å^{-1} along k_x. The topmost EDC in (a) has been fitted with an asymmetric peak because of the larger fwhm of the π-state in the $\bar{K}'$ valley and the Fermi level proximity. A reasonable fit with a symmetric peak could be achieved for the topmost peak in (b) because the fwhm of the π-state in the $\bar{K}$ valley is smaller and it does not cross the Fermi level. The spectra were measured after the external magnetic field application along $[0\bar{1}10]$ (M↑ in Figure 3). The peaks shown in gray can be attributed to the hybrid states of graphene/Au/Co(0001) since they are absent in the spectrum of pristine Co(0001).

the sample remagnetization (M↑), see Figure 3d,f. In this case, the giant spin splitting of 200 meV is observed at $\bar{K}'$, while a small one appears now at $\bar{K}$. As we show in Figure 3g, the π-state spin splitting lies in the range of 120−200 meV along the $\bar{K}'\bar{\Gamma}$ direction, at least up to $k_{\parallel} = -1.55$ Å^{-1}, which agrees with our ab initio calculations reported below.

We note again that the measurements at the $\bar{K}$ and $\bar{K}'$ points of the graphene BZ have been realized by a 180° azimuth angle rotation as it is shown in the insets in Figure 3c−g. Normal emission spectra of the Co d-bands (see Figure 5) show that the azimuth angle rotation by 180° is equivalent to the magnetization reversal. A turnover of the majority and minority Co bands upon the sample remagnetization (see transitions in Figure 5a → b and Figure 5c → d) is the same as that upon the azimuth angle sample rotation by 180° around the normal emission axis (see transitions in Figure 5a → c and Figure 5b → d).

To get further insights into a possible origin of this giant and asymmetric spin splitting, we have modeled a situation in which graphene bands overlap in wave vector and energy with well-defined spin-polarized Co states (see Supporting Information Note 4.3). Such a scenario cannot be excluded for example at the $\bar{K}$ and $\bar{K}'$ points, where the π-band could overlap with Co states, similar to those shown in Figure 1e,f. Assuming as an extreme case that graphene bands are only Rashba (and not exchange) split, we find that the summation of photoemission intensities of graphene bands and spin-polarized Co states also yields certain asymmetry in the apparent spin splitting values between the $\bar{K}'$ and $\bar{K}$ points. However, for a wide range of parameters the degree of this asymmetry is always much smaller than in the measurements. For example, setting graphene's Rashba splitting to 100 meV[25] and taking the separation between the Co states of 300 meV (as in Figure 1e,f), we obtain the spin splittings of 70 and 120 meV in the $\bar{K}'$ and $\bar{K}$ points, respectively. For comparison, Figure 1 (Figure 3) reports spin splittings of ∼0 and 150 (±20) meV (40 and 200 (±40) meV). Therefore, the asymmetric splitting that we find cannot be accounted for by a simple summation of intensities originated from Co spin-polarized and graphene's purely Rashba-split states: a coexistence of the Rashba and exchange splittings in the graphene bands is necessary to explain these observations.

Exchange Field Transfer Mechanism. Given the strong experimental indication of the combined action of the Rashba SOC and exchange field on the graphene π-states, we resort to DFT calculations to get insights into the mechanism of the magnetization transfer from the ferromagnetic substrate to graphene. As a first guess, we have neglected the Co−Au intermixing at the interface, but the joint Exchange+Rashba effect appeared to be marginal (Note B2 of the Supporting Information). In fact, a failure of such a model to describe the SOC and magnetization transfer might be indicative of the more complex crystal structure of our sample. Therefore, before continuing with further theoretical analysis, we have gone beyond the LEED characterization and acquired STM topographs. The latter have been found to depend drastically on the bias voltage. As one can see in Figure 6b, a well-known moiré structure of the Au-intercalated graphene[25,47,49] is observed for $V = 2$ mV. However, if the bias voltage is increased to, for example, 5 mV, a peculiar periodic pattern of the triangular-shaped features starts to be discernible (Figure 6a). The use of an intermediate V value of 3 mV allows one to visualize both the moiré and triangles patterns on the same topograph, c.f., the lower and upper halves of Figure 6c. Figure 6d shows the sharpest STM image of the triangular-shaped features pattern, obtained at $V = 10$ mV and $I = 0.4$ nA. Its period is measured to be ∼24−26 Å, as illustrated by the profile in Figure 6e, which corresponds to the $p(10 \times 10)$ superstructure determined by LEED shown in Figure 1a. Such STM results have been obtained on the scales up to 100 × 100 nm^2. We note that the variation of the applied bias voltage from 2 to 10 mV is accompanied by large (up to 3.5 Å) variation of the tip−sample distance s which justifies the change of appearance of the STM images shown in Figure 6. Only when large enough s values (equivalently, large enough V values) are used the triangular dislocation network is observed, although the precise threshold value of V for its observation is surprisingly low, that is, a few millivolts only. The physical explanation of these observations is that the Au/Co(0001) states close to the Fermi level have larger spatial extension perpendicular to the surface than the graphene states and, thus, only at large enough tip−sample distances the STM image shows better the triangular dislocation network with a minimal influence of graphene states. Indeed, Figure 6d shows the best resolution for the triangular dislocation network of the Au/Co(0001) system in the STM image taken at 10 mV, that is, at the largest tip−sample distance, with a rather blurred graphene on top of it. At $V = 5$ meV, magnification of the STM image between triangles reveals graphene's honeycomb lattice (Figure 6f).

It is worth noticing at this point, that the observed moiré pattern indicates the $p(10 \times 10)$ superstructure to hardly break the graphene A-B symmetry since the two sublattices are indistinguishable which excludes the opening of the DP gap of the structural origin. Moreover, as argued in ref 57, the formation of the spin−orbit gap is not expected in graphene when it is incommensurate with the substrate. These factors, together with the above-described ARPES indications, point toward the absence of the DP gap of any origin in our Au-intercalated graphene on Co(0001), which thus retains a quasi-freestanding character in this aspect.

DOI: 10.1021/acs.nanolett.7b01548
Nano Lett. 2018, 18, 1564−1574

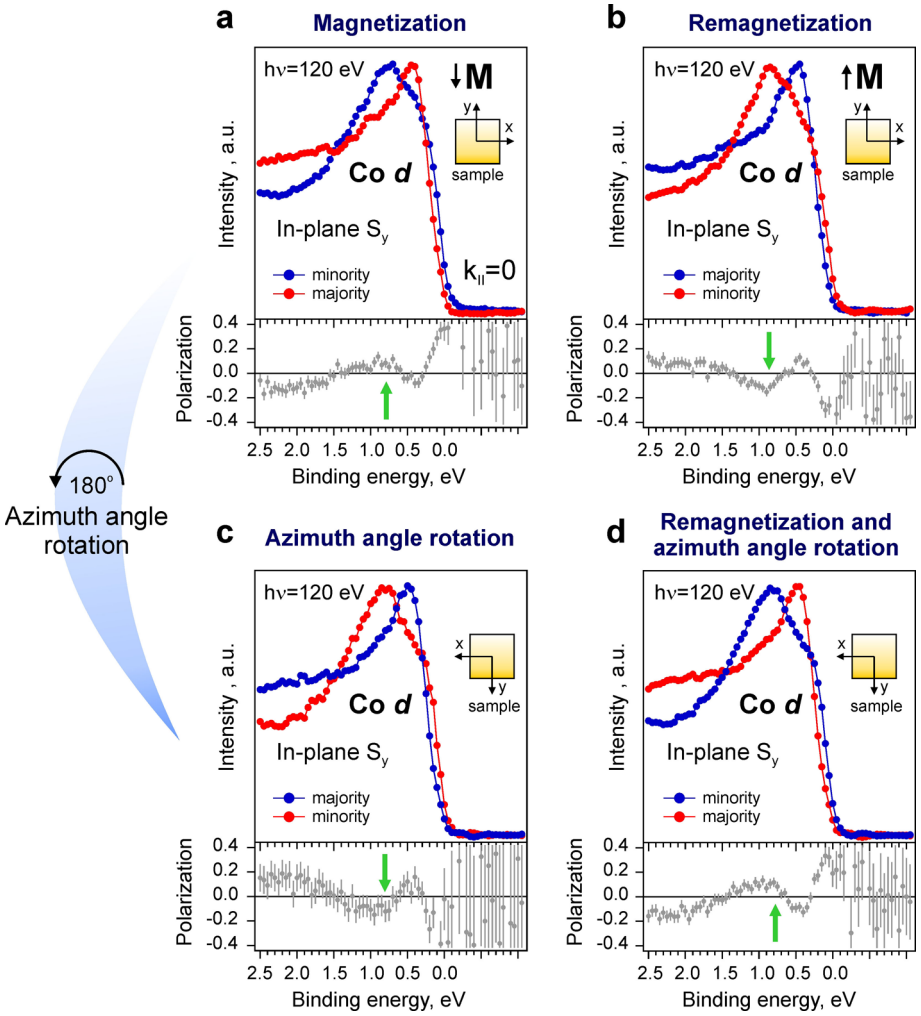

Figure 5. Spin-resolved photoemission spectra of the Co d-band for two geometries of the experiment. (a,b) Spin-resolved normal emission spectra of the Co d-band for graphene/Au/Co(0001) after magnetization and remagnetization, respectively. (c,d) The same spin-resolved spectra measured after a 180° rotation of the sample around the normal emission axis (azimuth angle rotation). Both panels a and c are measured after magnetization M↓, while panels b and d are measured after remagnetization M↑. The photon energy is 120 eV.

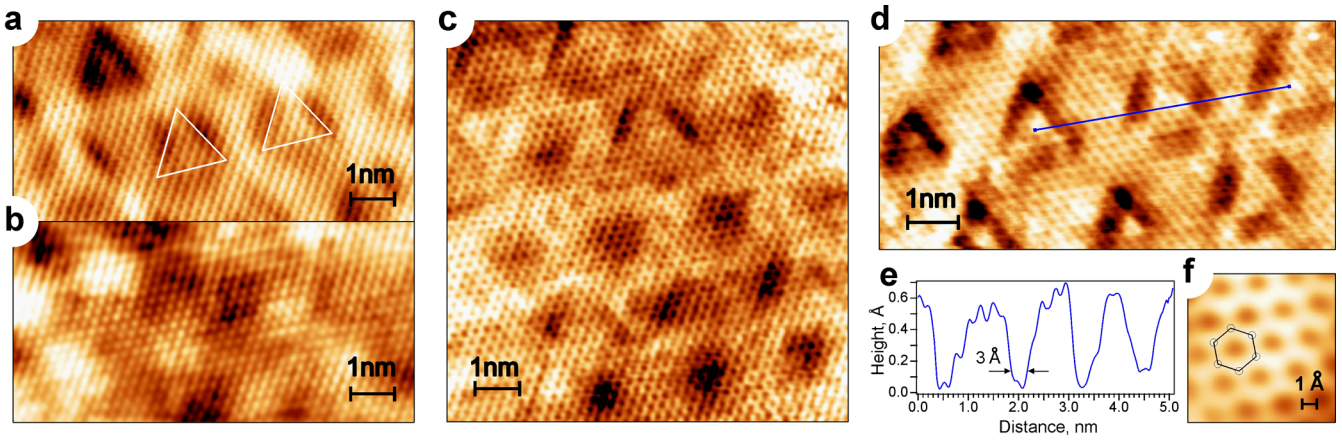

Figure 6. STM insight into the atomic structure of the graphene/Au/Co(0001) interfaces. (a,b) STM images (9×4.5 nm^2) acquired from the same area of the graphene/Au/Co(0001) sample using different bias voltages V: $V = 5$ mV, $I = 0.43$ nA (a) and $V = 2$ mV, $I = 0.43$ nA (b). (c) STM image (9×9 nm^2) obtained with $V = 3$ mV and $I = 0.4$ nA. (d,e) STM image (9.42×4.5 nm^2) of periodic triangular structure (scanning parameters $V = 10$ mV and $I = 0.4$ nA) with profile taken along the blue line. (f) A 1×1 nm^2 atomically resolved STM image ($V = 5$ mV and $I = 0.4$ nA).

A similar triangular-shaped pattern was previously seen by STM for a submonolayer of Au on Ni(111) with $p(9.7 \times 9.7)$ periodicity and dubbed "misfit dislocation loops".[58] It was found that periodic network of triangles, reflecting nothing but the structure at the buried Au/Ni(111) interface, appears due to the interface strain relief. At that, formation of each triangle requires

DOI: 10.1021/acs.nanolett.7b01548
Nano Lett. 2018, 18, 1564−1574

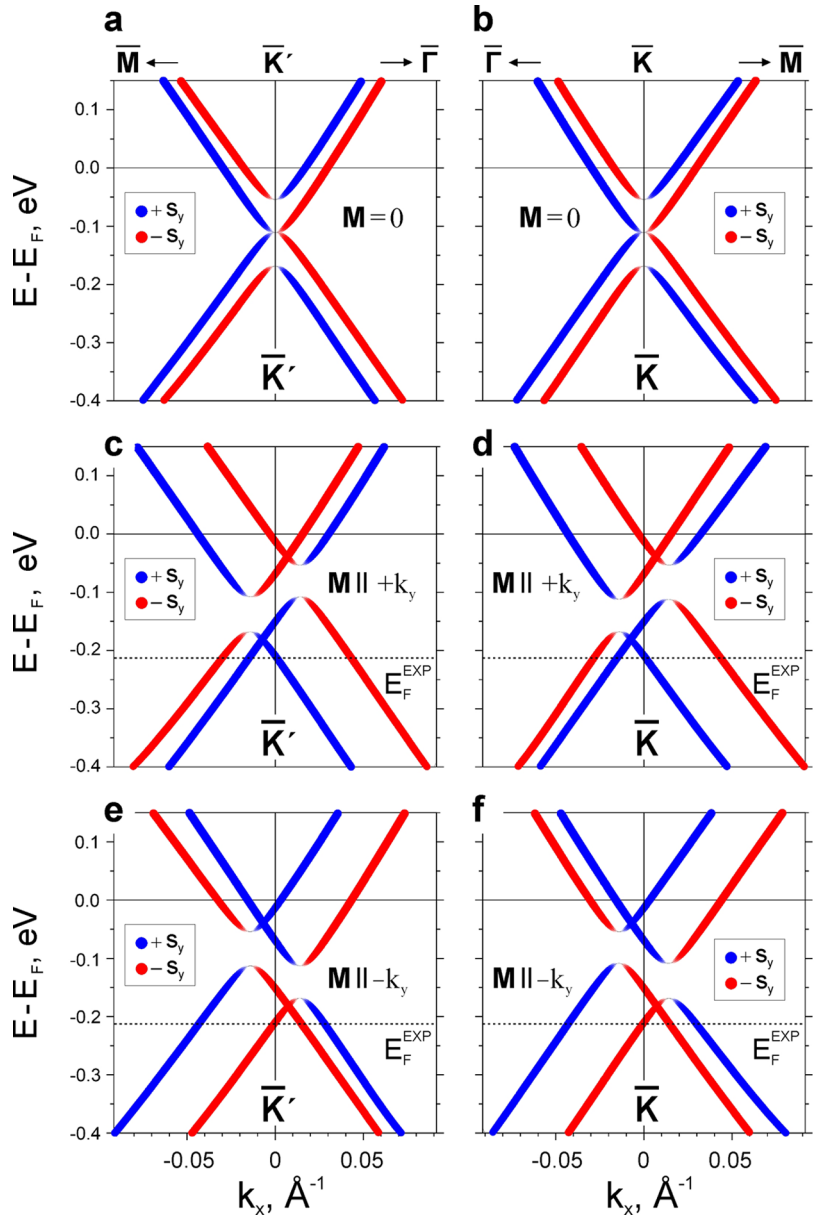

Figure 7. First-principles insight into dispersion and spin structure of graphene π-bands in the presence of Rashba SOC and in-plane exchange field. (a–f) Spin- and valley-resolved carbon-projected bandstructure of graphene/Au (a,b) without and (c–f) with constraining the magnetic moments on carbon atoms. The magnetization vector is directed along $+k_y$ ($-k_y$) in panels c,d (e,f). Left (right) panels show the bands in the ($\bar{K}'$) $\bar{K}$ valleys. The thickness of the color lines and the degree of their transparency reflect the module of the $\pm s_y$ spin projections.

squeezing several atoms from the interface Ni layer that turn out to be incorporated in the Au overlayer apparently as both isolated monomers and clusters, consisting of several atoms.[58] It was found in ref 58 that the number of Ni atoms squeezed out of the surface layer in order to form the underlying dislocation loops is equal to the number of Ni atoms incorporated into the Au layer. Turning back to the graphene/Au/Co system, we stress that it shows several close similarities to the Au/Ni(111) one. First, both the Co(0001) and Ni(111) surfaces are hexagonal and have similar lattice parameters. Second, as evidenced by STM, the periodicities of the systems' superstructures are very close: $p(10 \times 10)$ and $p(9.7 \times 9.7)$, respectively. Finally, both systems feature very similar periodic network of triangles. There is, of course, a principal difference between the two which is the presence of the graphene layer on top of Au/Co(0001). However, as it has been exemplified by the Pb-intercalated graphene/Ir(111),[30] Pb atoms form the same $c(4 \times 2)$ superstructure both being deposited on the pure Ir(111) surface and intercalated below graphene/Ir(111). These facts altogether strongly suggest that the Au/Co(0001) interface below graphene is the same as the one formed in the Au/Ni(111) without graphene,[58] which, in particular, means, that there are cobalt atoms incorporated in the Au layer. Unfortunately, the XPS analysis has not allowed us to detect any noticeable energy shift (more than 0.1 eV) of the Co 2p core level after the Au intercalation. A similar situation at the Au/Co interface has been reported in refs 59 and 60. As far as the valence band states are concerned, the Co d-peak measured at normal emission is widened after Au intercalation, which can be explained by the hybridization at the interface, while no noticeable energy shift of the peak is observed. We note that the absence of the Co core level and valence band states shifts upon Au-intercalation (at least within the experimental resolution)

DOI: 10.1021/acs.nanolett.7b01548
Nano Lett. 2018, 18, 1564–1574

does not exclude the presence of certain amount of Co atoms in the Au layer, as has been explained above on the basis of the triangular misfit dislocation model.[58] Therefore, one can suppose that the latter can open a channel of magnetization transfer from the substrate to graphene via direct cobalt−carbon hybridization.

A straightforward DFT calculation for the $p(10 \times 10)$ superstructure containing a network of triangular-shaped features revealed by our STM measurements is hardly possible. Therefore, to confirm that such an asymmetry of the π-state splitting may indeed stem from the exchange field and Rashba SOC joint action, the following calculation is performed. We effectively take into account the exchange field transfer that the formation of the triangular-shaped features network is expected to facilitate by applying a magnetization constraint to the graphene sheet placed on top of the gold layer (see Methods for geometry description). Figure 7a,b shows the calculated in the $\bar{K}$ and $\bar{K}'$ valleys graphene-projected bandstructure with only SOC included (i.e., for a zero exchange field). In this case, the Rashba-type spin splitting of the Dirac cone[28] is expectedly revealed, the Rashba parameter λ being equal to 57 meV. If an exchange field is then introduced parallel to $+k_y$, a magnetic moment of ~0.002 μ_B is fixed on each carbon atom (as calculated within a Wigner-Seitz sphere; the exchange splitting of the Dirac cone is ~140 meV), an asymmetric splitting develops along k_x in perfect agreement with our experiment, reaching a giant value of 175 meV near $\bar{K}'$ along $\bar{\Gamma}\bar{K}'$ (Figure 7c), but only of 53 meV near $\bar{K}$ along $\bar{\Gamma}\bar{K}$ (Figure 7d). On the other hand, upon remagnetization, a giant (moderate) splitting is observed along the $\bar{\Gamma}\bar{K}$ ($\bar{\Gamma}\bar{K}'$) direction (Figure 7e,f). The π-states dispersion presented in Figure 7 agrees qualitatively with that obtained within the model Hamiltonian approach.[15] Note that although the resulting magneto-spin−orbit graphene dispersion shows local gaps in the $\bar{K}$ and $\bar{K}'$ points, the global gap between the π and π^* bands is absent.

It should also be noted that choosing the graphene adsorption height of 2.65 Å and a magnetic moment value of 0.002 μ_B per C atom provides the calculated splitting values in the best agreement with the experimental ones. This adsorption distance can be interpreted as an average graphene-Au distance taking into account the corrugation shown in Figures 6d,e. The latter is expected to enable a Co-3d-C-2p hybridization leading to magnetization of graphene. We would also like to note that only ~0.002 μ_B per carbon atom is needed to achieve giant splitting of 175 meV. This value is an order of magnitude smaller than that induced on C atoms in graphene/Co (i.e., without Au). Taking into account that the intercalated layer of graphene/Au/Co is essentially Au-rich, this magnitude of the carbon magnetization appears to be quite realistic, although suggesting predominantly ferromagnetic alignment of the local moments of the Co atoms incorporated in the Au layer. According to our exchange coupling parameters calculations, this ferromagnetic alignment is expected to be stabilized due to the strong exchange interactions with the local moments of the substrate Co atoms (Note B4 of the Supporting Information). Indeed, the strongest interactions, involving the incorporated Co atoms, are characterized by positive exchange integrals and correspond to the coupling with the nearest neighbors from the Co substrate. As a result, the moments of the incorporated Co atoms are indeed expected to be ferromagnetically ordered to the magnetization of the substrate. Moreover, since the maximal exchange integrals obtained are of the same order of magnitude or even up to two times larger than those in, for example, the bulk iron, such an ordering can be stable up to the room or even higher temperature.

Thus, using angle- and spin-resolved photoemission spectroscopy, scanning tunneling microscopy and density functional theory calculations, we have evidenced an emergence of a new dimension of the quasi-freestanding graphene's functionality, a combination of robust magnetism and strong spin−orbit coupling. This magneto-spin−orbit version of graphene is achieved owing to peculiar blend of the Co film in-plane magnetization, strong spin−orbit coupling of the intercalated gold layer and reconstruction of the hidden Au/Co(0001) interface. Altogether, these factors give rise to a very high, 0.2 eV spin splitting of the graphene Dirac cone without loss of its linear dispersion which is a major step toward achievement of graphene-based spintronics. To be specific, our results pave a way to phenomena, that rely on the graphene's bandstructure resulting from the Rashba spin−orbit splitting and in-plane magnetism, for example, the optical generation of a spin-polarized current[15] or spin−orbit torque.[13] Crucially for these phenomena, the high Curie point of cobalt guarantees the magnetism-derived properties of the system to persist above room temperature. In a fundamental aspect, our results give rise to new exciting possibilities for this novel bandstructure of graphene. Apart from the obvious need of its further study per se, the observed bandstructure can subsequently be tuned to enable, for example, a bandgap engineering by a selective doping of graphene[46] or a quantum-anomalous-Hall-like state by choosing a thicker Co substrate that would feature an out-of-plane magnetization.

Methods. Spin- and angle-resolved photoemission experiments were performed at the resource center "Physical methods of surface investigation" (PMSI) of Research park of Saint Petersburg State University at the research modular platform Nanolab. A hemispherical energy analyzer VG Scienta R4000 equipped with a 25 kV 3D Mott polarimeter and a narrowband high-intensity UV He-discharge ($h\nu$ = 21.2 eV) light source Scienta VUV 5k with retractable capillary (⌀ 0.8 mm) were used. The energy and angular resolutions were 17 meV and 0.5° (143 meV and 3°), respectively, for ARPES (spin-ARPES). All spin-ARPES measurements are shown in the coordinate system of the 3D Mott detector, which for the measured emission angles coincides with the sample coordinate system, except for the sample rotation by 180° around the normal. In this case, the directions of the s_x and s_y axes in the sample coordinate system become oppositely directed to corresponding axes in the detector coordinate system. It should also be noted that only in-plane s_y spin polarization data are presented in the main text. XPS measurements were performed using monochromated Al K_α radiation (the energy resolution was 0.45 eV). Low-energy electron diffraction patterns were obtained with diffractometer OCI BDL800IR. Part of the ARPES and spin-ARPES experiments were done at the U125-2_SGM, UE56-2_PGM-2 beamlines at Helmholtz-Zentrum Berlin (BESSY II) using a p-polarized synchrotron radiation at experimental station Phoenexs employing a hemispherical energy analyzer SPECS Phoibos 150 equipped with a 26 kV 2D Mott polarimeter (the energy and angular resolutions were 150 meV for ARPES, 100 meV for spin-ARPES and 1° for both methods). The analysis procedure for the spin-ARPES data is described in Note A5 of the Supporting Information. STM measurements were performed at the PMSI using a UHV module of the scanning tunneling and atomic force microscope Omicron VT AFM XA 50/500. All ARPES and STM measurements were carried out at room temperature. The samples were synthesized at the PMSI. Well-oriented graphene was prepared by chemical vapor deposition on the previously annealed Co(95 Å)/W(110) surface at temperature of 660°.[45]

DOI: 10.1021/acs.nanolett.7b01548
Nano Lett. 2018, 18, 1564−1574

The intercalation of the Au monolayer was done by a deposition of gold atoms (3.6 Å or ∼1.5 monolayers) on graphene/Co(0001)/W(110), followed by annealing at temperatures 450−500°. Co film was magnetized by a current pulse through the coils close to the sample. Peak value of the applied magnetic field at the sample position and decay time were 0.3 T and ∼0.2 ms, respectively.

Electronic structure calculations were carried out within DFT using the projector augmented-wave method[61] as implemented in the VASP code.[62,63] The exchange-correlation energy was treated using the generalized gradient approximation.[64] The Hamiltonian contained the scalar relativistic corrections and the spin−orbit coupling was taken into account by the second variation method.[65] In order to describe the van der Waals interactions we made use of the DFT-D3[66,67] approach. The energy cutoff for the plane-wave expansion was set to 400 eV. All calculations were performed using a $\bar{\Gamma}$-centered k-point grid of 21 × 21 × 1 in the two-dimensional Brillouin zone.

We used a model of repeating slabs separated by a vacuum gap of a minimum of 10 Å. As a structural model of our graphene/Au/Co(0001) system, showing $p(10 \times 10)$ periodicity, we adopted a simplified one that was employed in ref 68 for a similar graphene/Au/Ni(111) system. It assumes that the intercalated gold atoms are arranged in the $(\sqrt{3} \times \sqrt{3})$R30° periodicity that is commensurate with both the graphene's and cobalt's (2×2) cell (Figure S17 of the Supporting Information). In the supercell, the three gold atoms are placed in such a way that one of them falls into the honeycomb's hollow site, another one lies exactly below one of the A-sublattice carbon atoms, while the last one lies below one of the B-subblatice sites. With respect to Co, the intercalated layer resides such that the three gold atoms are located in the on-top, fcc, and hcp hollows of the (0001) surface. Graphene is commensurate with Co(0001) and is placed in the fcc-top registry.[46] The in-plane lattice parameter of Co(0001) was set to 2.507 Å. By choosing this structural model we compromise between the system's treatability within DFT on the one hand, because a $p(10 \times 10)$ cell study would require a vast computational effort, and the conservation of its basic structural characteristics on the other hand. Indeed, the model basically captures the presence of Au atoms that are located at different positions with respect to graphene and describes satisfactorily the average Au−Au next neighbor distance (∼2.9 Å vs 2.75 Å in the experiment). The Co film thickness was chosen to be five atomic layers and all the interlayer distances were optimized using a conjugate-gradient algorithm and a force tolerance criterion for convergence of 0.03 eV/Å (spin−orbit coupling was included during the relaxation). The electronic structure calculated for the geometry obtained is shown in Figure S17.

As an alternative way to account for graphene's magnetization, we applied a magnetic moment constraint (constrained DFT calculation) to the carbon atoms using the above-described structural model, but with removed Co substrate. The graphene sheet magnetization magnitude and the graphene−Au interlayer distance (controlling the induced SOC strength) were treated as the parameters that were varied in the physically meaningful ranges to achieve the spin splitting values obtained in our experiments. At that, the graphene and gold layers were maintained planar. The bandstructures for this case are shown in Figure 7.

The exchange coupling constants have been computed using the magnetic force theorem as it is implemented within the multiple scattering theory.[69] This method provides the exchange parameters entering the Heisenberg model from the energy change induced by an infinitesimal rotation of the magnetic moments. For calculations, we have used a full potential fully relativistic Green function method, specially designed for surfaces and interfaces.[70,71] The structural model employed in the calculation is described in details in the Note B4 of the Supporting Information.

■ ASSOCIATED CONTENT

Supporting Information

The Supporting Information is available free of charge on the ACS Publications website at DOI: 10.1021/acs.nanolett.7b01548.

Additional experimental and theoretical results are presented on electronic and crystal structures of graphene/Co(0001)/W(110); Au intercalation verification; ARPES and spin-ARPES data for graphene/Au/Co(0001)/W(110) taken by polar angle variation; analysis of the sample magnetization; spin-ARPES data for Co(0001)/W(110) and Au(1 ML)/Co(0001)/W(110); procedure of spin-resolved ARPES data analysis; spin-ARPES data with s_x+s_z polarization for graphene/Au/Co(0001)/W(110); theoretical insights into the magneto-spin−orbit graphene electronic structure; ab initio calculations of the exchange coupling constants for the graphene/Au/Co(0001) system (PDF)

■ AUTHOR INFORMATION

Corresponding Author

*E-mail: artem.rybkin@spbu.ru.

ORCID

Artem G. Rybkin: 0000-0002-8237-4959
Oleg Yu. Vilkov: 0000-0002-8984-8790
Ilya I. Klimovskikh: 0000-0003-0243-0322
Anatoly E. Petukhov: 0000-0001-9362-3589

Notes

The authors declare no competing financial interest.

■ ACKNOWLEDGMENTS

M.M.O. and A.A. acknowledge useful discussions with J. I. Cerdá, F. Schiller, and J. E. Ortega. The authors acknowledge support by the Saint Petersburg State University (Grant 15.61.202.2015), German-Russian Interdisciplinary Science Center (G-RISC) funded by the German Federal Foreign Office via the German Academic Exchange Service (DAAD) and Russian-German laboratory at BESSY II (Helmholtz-Zentrum Berlin). The funding by the University of the Basque Country (Grants GIC07IT36607 and IT-756-13), the Spanish Ministry of Science and Innovation (Grants FIS2013-48286-C02-02-P, FIS2013-48286-C02-01-P, and FIS2016-75862-P) and Tomsk State University competitiveness improvement programme (Project No. 8.1.01.2017) is also gratefully acknowledged. I.P.R. acknowledges support by the Ministry of Education and Science of the Russian Federation within the framework of the governmental program "Megagrants" (state task no. 3.8895.2017/P220). The calculations were performed in the Donostia International Physics Center and the Computing Center (Research Park of Saint Petersburg State University (http://cc.spbu.ru).

■ REFERENCES

(1) Castro Neto, A. H.; Guinea, F.; Peres, N. M. R.; Novoselov, K. S.; Geim, A. K. The electronic properties of graphene. *Rev. Mod. Phys.* **2009**, *81*, 109.

(2) Yazyev, O. V. Emergence of magnetism in graphene materials and nanostructures. *Rep. Prog. Phys.* **2010**, 73, 056501.

DOI: 10.1021/acs.nanolett.7b01548
Nano Lett. 2018, 18, 1564−1574

(3) Pesin, D.; MacDonald, A. H. Spintronics and pseudospintronics in graphene and topological insulators. *Nat. Mater.* **2012**, *11*, 409−416.
(4) Han, W.; Kawakami, R. K.; Gmitra, M.; Fabian, J. Graphene spintronics. *Nat. Nanotechnol.* **2014**, *9*, 794−807.
(5) Ferrari, A. C.; Bonaccorso, F.; Fal'ko, V.; Novoselov, K. S.; Roche, S.; Bøggild, P.; Borini, S.; Koppens, F. H. L.; Palermo, V.; Pugno, N.; Garrido, J. A.; Sordan, R.; Bianco, A.; Ballerini, L.; Prato, M.; Lidorikis, E.; Kivioja, J.; Marinelli, C.; Ryhänen, T.; Morpurgo, A.; Coleman, J. N.; Nicolosi, V.; Colombo, L.; Fert, A.; Garcia-Hernandez, M.; Bachtold, A.; Schneider, G. F.; Guinea, F.; Dekker, C.; Barbone, M.; Sun, Z.; Galiotis, C.; Grigorenko, A. N.; Konstantatos, G.; Kis, A.; Katsnelson, M.; Vandersypen, L.; Loiseau, A.; Morandi, V.; Neumaier, D.; Treossi, E.; Pellegrini, V.; Polini, M.; Tredicucci, A.; Williams, G. M.; Hee Hong, B.; Ahn, J.-H.; Min Kim, J.; Zirath, H.; van Wees, B. J.; van der Zant, H.; Occhipinti, L.; Di Matteo, A.; Kinloch, I. A.; Seyller, T.; Quesnel, E.; Feng, X.; Teo, K.; Rupesinghe, N.; Hakonen, P.; Neil, S. R. T.; Tannock, Q.; Löfwander, T.; Kinaret, J. Science and technology roadmap for graphene, related two-dimensional crystals, and hybrid systems. *Nanoscale* **2015**, *7*, 4598−4810.
(6) Roche, S.; Åkerman, J.; Beschoten, B.; Charlier, J.-C.; Chshiev, M.; Dash, S. P.; Dlubak, B.; Fabian, J.; Fert, A.; Guimarães, M.; Guinea, F.; Grigorieva, I.; Schönenberger, C.; Seneor, P.; Stampfer, C.; Valenzuela, S. O.; Waintal, X.; van Wees, B. Graphene spintronics: the European Flagship perspective. *2D Mater.* **2015**, *2*, 030202.
(7) Balakrishnan, J.; Koon, G. K. W.; Jaiswal, M.; Castro Neto, A. H.; Özyilmaz, B. Colossal enhancement of spin-orbit coupling in weakly hydrogenated graphene. *Nat. Phys.* **2013**, *9*, 284−287.
(8) Kane, C. L.; Mele, E. J. Quantum Spin Hall Effect in Graphene. *Phys. Rev. Lett.* **2005**, *95*, 226801.
(9) Semenov, Y. G.; Kim, K. W.; Zavada, J. M. Spin field effect transistor with a graphene channel. *Appl. Phys. Lett.* **2007**, *91*, 153105.
(10) Zhou, B.; Chen, X.; Wang, H.; Ding, K.-H.; Zhou, G. Magnetotransport and current-induced spin transfer torque in a ferromagnetically contacted graphene. *J. Phys.: Condens. Matter* **2010**, *22*, 445302.
(11) Yang, H. X.; Hallal, A.; Terrade, D.; Waintal, X.; Roche, S.; Chshiev, M. Proximity Effects Induced in Graphene by Magnetic Insulators: First-Principles Calculations on Spin Filtering and Exchange-Splitting Gaps. *Phys. Rev. Lett.* **2013**, *110*, 046603.
(12) Qiao, Z.; Yang, S. A.; Feng, W.; Tse, W.-K.; Ding, J.; Yao, Y.; Wang, J.; Niu, Q. Quantum anomalous Hall effect in graphene from Rashba and exchange effects. *Phys. Rev. B: Condens. Matter Mater. Phys.* **2010**, *82*, 161414.
(13) Dyrdał, A.; Barnaś, J. Current-induced spin polarization and spin-orbit torque in graphene. *Phys. Rev. B: Condens. Matter Mater. Phys.* **2015**, *92*, 165404.
(14) Shikin, A. M.; Rybkina, A. A.; Rybkin, A. G.; Klimovskikh, I. I.; Skirdkov, P. N.; Zvezdin, K. A.; Zvezdin, A. K. Spin current formation at the graphene/Pt interface for magnetization manipulation in magnetic nanodots. *Appl. Phys. Lett.* **2014**, *105*, 042407.
(15) Inglot, M.; Dugaev, V. K.; Sherman, E. Y.; Barnaś, J. Enhanced photogalvanic effect in graphene due to Rashba spin-orbit coupling. *Phys. Rev. B: Condens. Matter Mater. Phys.* **2015**, *91*, 195428.
(16) Novoselov, K. S.; Geim, A. K.; Morozov, S. V.; Jiang, D.; Zhang, Y.; Dubonos, S. V.; Grigorieva, I. V.; Firsov, A. A. Electric field effect in atomically thin carbon films. *Science* **2004**, *306*, 666−669.
(17) Novoselov, K. S.; Geim, A. K.; Morozov, S. V.; Jiang, D.; Katsnelson, M. I.; Grigorieva, I. V.; Dubonos, S. V.; Firsov, A. A. Two-dimensional gas of massless Dirac fermions in graphene. *Nature* **2005**, *438*, 197.
(18) Geim, A. K.; Novoselov, K. S. The rise of graphene. *Nat. Mater.* **2007**, *6*, 183.
(19) Farmer, D. B.; Chiu, H.-Y.; Lin, Y.-M.; Jenkins, K. A.; Xia, F.; Avouris, P. Utilization of a buffered dielectric to achieve high field-effect carrier mobility in graphene transistors. *Nano Lett.* **2009**, *9*, 4474−4478.
(20) Xia, F.; Farmer, D. B.; Lin, Y.-m.; Avouris, P. Graphene field-effect transistors with high on/off current ratio and large transport band gap at room temperature. *Nano Lett.* **2010**, *10*, 715−718.
(21) Avsar, A.; Tan, J. Y.; Taychatanapat, T.; Balakrishnan, J.; Koon, G.; Yeo, Y.; Lahiri, J.; Carvalho, A.; Rodin, A.; O'Farrell, E.; Eda, G.; Castro Neto, A.; Özyilmaz, B. Spin−orbit proximity effect in graphene. *Nat. Commun.* **2014**, *5*, 4875.
(22) Avsar, A.; Lee, J. H.; Koon, G. K. W.; Özyilmaz, B. Enhanced spin-orbit coupling in dilute fluorinated graphene. *2D Mater.* **2015**, *2*, 044009.
(23) Gruber, E.; Wilhelm, R. A.; Pétuya, R.; Smejkal, V.; Kozubek, R.; Hierzenberger, A.; Bayer, B. C.; Aldazabal, I.; Kazansky, A. K.; Libisch, F.; Krasheninnikov, A. V.; Schleberger, M.; Facsko, S.; Borisov, A. G.; Arnau, A.; Aumayr, F. Ultrafast electronic response of graphene to a strong and localized electric field. *Nat. Commun.* **2016**, *7*, 13948.
(24) Klimovskikh, I. I.; Tsirkin, S. S.; Rybkin, A. G.; Rybkina, A. A.; Filianina, M. V.; Zhizhin, E. V.; Chulkov, E. V.; Shikin, A. M. Nontrivial spin structure of graphene on Pt(111) at the Fermi level due to spin-dependent hybridization. *Phys. Rev. B: Condens. Matter Mater. Phys.* **2014**, *90*, 235431.
(25) Marchenko, D.; Varykhalov, A.; Scholz, M. R.; Bihlmayer, G.; Rashba, E. I.; Rybkin, A.; Shikin, A. M.; Rader, O. Giant Rashba splitting in graphene due to hybridization with gold. *Nat. Commun.* **2012**, *3*, 1232.
(26) Shikin, A. M.; Rybkin, A. G.; Marchenko, D.; Rybkina, A. A.; Scholz, M. R.; Rader, O.; Varykhalov, A. Induced spin-orbit splitting in graphene: the role of atomic number of the intercalated metal and π−d hybridization. *New J. Phys.* **2013**, *15*, 013016.
(27) Varykhalov, A.; Sánchez-Barriga, J.; Marchenko, D.; Hlawenka, P.; Mandal, P.; Rader, O. Tunable Fermi level and hedgehog spin texture in gapped graphene. *Nat. Commun.* **2015**, *6*, 7610.
(28) Rashba, E. I. Graphene with structure-induced spin-orbit coupling: Spin-polarized states, spin zero modes, and quantum Hall effect. *Phys. Rev. B: Condens. Matter Mater. Phys.* **2009**, *79*, 161409.
(29) Gmitra, M.; Konschuh, S.; Ertler, C.; Ambrosch-Draxl, C.; Fabian, J. Band-structure topologies of graphene: Spin-orbit coupling effects from first principles. *Phys. Rev. B: Condens. Matter Mater. Phys.* **2009**, *80*, 235431.
(30) Calleja, F.; Ochoa, H.; Garnica, M.; Barja, S.; Navarro, J. J.; Black, A.; Otrokov, M. M.; Chulkov, E. V.; Arnau, A.; de Parga, A. L. V.; Guinea, F.; Miranda, R. Spatial variation of a giant spin-orbit effect induces electron confinement in graphene on Pb islands. *Nat. Phys.* **2015**, *11*, 43−47.
(31) Klimovskikh, I. I.; Otrokov, M. M.; Voroshnin, V. Y.; Sostina, D.; Petaccia, L.; Di Santo, G.; Thakur, S.; Chulkov, E. V.; Shikin, A. M. Spin-Orbit Coupling Induced Gap in Graphene on Pt(111) with Intercalated Pb Monolayer. *ACS Nano* **2017**, *11*, 368−374.
(32) Varykhalov, A.; Rader, O. Graphene grown on Co(0001) films and islands: Electronic structure and its precise magnetization dependence. *Phys. Rev. B: Condens. Matter Mater. Phys.* **2009**, *80*, 035437.
(33) Rader, O.; Varykhalov, A.; Sánchez-Barriga, J.; Marchenko, D.; Rybkin, A.; Shikin, A. M. Is There a Rashba Effect in Graphene on 3*d* Ferromagnets? *Phys. Rev. Lett.* **2009**, *102*, 057602.
(34) Dedkov, Y. S.; Fonin, M. Electronic and magnetic properties of the grapheme−ferromagnet interface. *New J. Phys.* **2010**, *12*, 125004.
(35) Sánchez-Barriga, J.; Varykhalov, A.; Scholz, M.; Rader, O.; Marchenko, D.; Rybkin, A.; Shikin, A.; Vescovo, E. Chemical vapour deposition of graphene on Ni(111) and Co(0001) and intercalation with Au to study Dirac-cone formation and Rashba splitting. *Diamond Relat. Mater.* **2010**, *19*, 734.
(36) Marchenko, D.; Varykhalov, A.; Sánchez-Barriga, J.; Rader, O.; Carbone, C.; Bihlmayer, G. Highly spin-polarized Dirac fermions at the graphene/Co interface. *Phys. Rev. B: Condens. Matter Mater. Phys.* **2015**, *91*, 235431.
(37) Yazyev, O. V.; Helm, L. Defect-induced magnetism in graphene. *Phys. Rev. B: Condens. Matter Mater. Phys.* **2007**, *75*, 125408.
(38) Červenka, J.; Katsnelson, M.; Flipse, C. Room-temperature ferromagnetism in graphite driven by two-dimensional networks of point defects. *Nat. Phys.* **2009**, *5*, 840−844.
(39) Ugeda, M. M.; Brihuega, I.; Guinea, F.; Gómez-Rodríguez, J. M. Missing Atom as a Source of Carbon Magnetism. *Phys. Rev. Lett.* **2010**, *104*, 096804.

DOI: 10.1021/acs.nanolett.7b01548
Nano Lett. 2018, 18, 1564−1574

(40) Nair, R.; Sepioni, M.; Tsai, I.-L.; Lehtinen, O.; Keinonen, J.; Krasheninnikov, A.; Thomson, T.; Geim, A.; Grigorieva, I. Spin-half paramagnetism in graphene induced by point defects. *Nat. Phys.* **2012**, *8*, 199−202.
(41) González-Herrero, H.; Gómez-Rodríguez, J. M.; Mallet, P.; Moaied, M.; Palacios, J. J.; Salgado, C.; Ugeda, M. M.; Veuillen, J.-Y.; Yndurain, F.; Brihuega, I. Atomic-scale control of graphene magnetism by using hydrogen atoms. *Science* **2016**, *352*, 437−441.
(42) Boukhvalov, D. W.; Katsnelson, M. I.; Lichtenstein, A. I. Hydrogen on graphene: Electronic structure, total energy, structural distortions and magnetism from first-principles calculations. *Phys. Rev. B: Condens. Matter Mater. Phys.* **2008**, *77*, 035427.
(43) Hong, X.; Zou, K.; Wang, B.; Cheng, S.-H.; Zhu, J. Evidence for Spin-Flip Scattering and Local Moments in Dilute Fluorinated Graphene. *Phys. Rev. Lett.* **2012**, *108*, 226602.
(44) Giesbers, A. J. M.; Uhlířová, K.; Konečný, M.; Peters, E. C.; Burghard, M.; Aarts, J.; Flipse, C. F. J. Interface-Induced Room-Temperature Ferromagnetism in Hydrogenated Epitaxial Graphene. *Phys. Rev. Lett.* **2013**, *111*, 166101.
(45) Usachov, D.; Fedorov, A.; Otrokov, M. M.; Chikina, A.; Vilkov, O.; Petukhov, A.; Rybkin, A. G.; Koroteev, Y. M.; Chulkov, E. V.; Adamchuk, V. K.; Grüneis, A.; Laubschat, C.; Vyalikh, D. V. Observation of Single-Spin Dirac Fermions at the Graphene/Ferromagnet Interface. *Nano Lett.* **2015**, *15*, 2396−2401.
(46) Usachov, D. Y.; Fedorov, A. V.; Vilkov, O. Y.; Petukhov, A. E.; Rybkin, A. G.; Ernst, A.; Otrokov, M. M.; Chulkov, E. V.; Ogorodnikov, I. I.; Kuznetsov, M. V.; Yashina, L. V.; Kataev, E. Y.; Erofeevskaya, A. V.; Voroshnin, V. Y.; Adamchuk, V. K.; Laubschat, C.; Vyalikh, D. V. Large-Scale Sublattice Asymmetry in Pure and Boron-Doped Graphene. *Nano Lett.* **2016**, *16*, 4535−4543.
(47) Varykhalov, A.; Sánchez-Barriga, J.; Shikin, A. M.; Biswas, C.; Vescovo, E.; Rybkin, A.; Marchenko, D.; Rader, O. Electronic and Magnetic Properties of Quasifreestanding Graphene on Ni. *Phys. Rev. Lett.* **2008**, *101*, 157601.
(48) Usachov, D. Y.; Fedorov, A. V.; Petukhov, A. E.; Vilkov, O. Y.; Rybkin, A. G.; Otrokov, M. M.; Arnau, A.; Chulkov, E. V.; Yashina, L. V.; Farjam, M.; Adamchuk, V. K.; Senkovskiy, B. V.; Laubschat, C.; Vyalikh, D. V. Epitaxial B-Graphene: Large-Scale Growth and Atomic Structure. *ACS Nano* **2015**, *9*, 7314−7322.
(49) Varykhalov, A.; Scholz, M. R.; Kim, T. K.; Rader, O. Effect of noble-metal contacts on doping and band gap of graphene. *Phys. Rev. B: Condens. Matter Mater. Phys.* **2010**, *82*, 121101.
(50) Bostwick, A.; Ohta, T.; McChesney, J. L.; Emtsev, K. V.; Seyller, T.; Horn, K.; Rotenberg, E. Symmetry breaking in few layer graphene films. *New J. Phys.* **2007**, *9*, 385.
(51) Mucha-Kruczyński, M.; Tsyplyatyev, O.; Grishin, A.; McCann, E.; Fal'ko, V. I.; Bostwick, A.; Rotenberg, E. Characterization of graphene through anisotropy of constant-energy maps in angle-resolved photoemission. *Phys. Rev. B: Condens. Matter Mater. Phys.* **2008**, *77*, 195403.
(52) Krupin, O.; Bihlmayer, G.; Starke, K.; Gorovikov, S.; Prieto, J.; Döbrich, K.; Blügel, S.; Kaindl, G. Rashba effect at magnetic metal surfaces. *Phys. Rev. B: Condens. Matter Mater. Phys.* **2005**, *71*, 201403.
(53) Kaya, S. On the magnetization of single crystals of cobalt. *Sci. Rep. Tohoku Imp. Univ.* **1928**, *17*, 1157.
(54) Pinkvos, H.; Poppa, H.; Bauer, E.; Hurst, J. Spin-polarized low-energy electron microscopy study of the magnetic microstructure of ultra-thin epitaxial cobalt films on W(110). *Ultramicroscopy* **1992**, *47*, 339−345.
(55) Getzlaff, M.; Bansmann, J.; Braun, J.; Schönhense, G. Spin resolved photoemission study of Co(0001) films. *J. Magn. Magn. Mater.* **1996**, *161*, 70−88.
(56) Hartmann, D.; Weber, W.; Wesner, D.; Popovic, S.; Güntherodt, G. Spin-polarized photoemission at interfaces of noble metals with Co and Fe. *J. Magn. Magn. Mater.* **1993**, *121*, 160−162.
(57) Brey, L. Spin-orbit coupling in graphene induced by adatoms with outer-shell *p* orbitals. *Phys. Rev. B: Condens. Matter Mater. Phys.* **2015**, *92*, 235444.
(58) Besenbacher, F. Scanning tunnelling microscopy studies of metal surfaces. *Rep. Prog. Phys.* **1996**, *59*, 1737−1802.
(59) Mamy, R. Growth of Co on Au(111): a photoemission study. *Surf. Sci.* **1995**, *322*, 337−341.
(60) Prieto, M. J.; Carbonio, E. A.; Landers, R.; de Siervo, A. Structural and electronic characterization of Co nanostructures on Au(332). *Surf. Sci.* **2013**, *617*, 87−93.
(61) Blöchl, P. E. Projector augmented-wave method. *Phys. Rev. B: Condens. Matter Mater. Phys.* **1994**, *50*, 17953−17979.
(62) Kresse, G.; Furthmüller, J. Efficient iterative schemes for ab initio total-energy calculations using a plane-wave basis set. *Phys. Rev. B: Condens. Matter Mater. Phys.* **1996**, *54*, 11169−11186.
(63) Kresse, G.; Joubert, D. From ultrasoft pseudopotentials to the projector augmented-wave method. *Phys. Rev. B: Condens. Matter Mater. Phys.* **1999**, *59*, 1758−1775.
(64) Perdew, J. P.; Burke, K.; Ernzerhof, M. Generalized Gradient Approximation Made Simple. *Phys. Rev. Lett.* **1996**, *77*, 3865−3868.
(65) Koelling, D. D.; Harmon, B. N. A technique for relativistic spin-polarised calculations. *J. Phys. C: Solid State Phys.* **1977**, *10*, 3107.
(66) Grimme, S.; Antony, J.; Ehrlich, S.; Krieg, H. A consistent and accurate ab initio parametrization of density functional dispersion correction (DFT-D) for the 94 elements H-Pu. *J. Chem. Phys.* **2010**, *132*, 154104.
(67) Grimme, S.; Ehrlich, S.; Goerigk, L. Effect of the damping function in dispersion corrected density functional theory. *J. Comput. Chem.* **2011**, *32*, 1456−1465.
(68) Kang, M. H.; Jung, S. C.; Park, J. W. Density functional study of the Au-intercalated graphene/Ni(111) surface. *Phys. Rev. B: Condens. Matter Mater. Phys.* **2010**, *82*, 085409.
(69) Liechtenstein, A. I.; Katsnelson, M. I.; Antropov, V. P.; Gubanov, V. A. Local spin density functional approach to the theory of exchange interactions in ferromagnetic metals and alloys. *J. Magn. Magn. Mater.* **1987**, *67*, 65−74.
(70) Lüders, M.; Ernst, A.; Temmerman, W. M.; Szotek, Z.; Durham, P. J. Ab initio angle-resolved photoemission in multiple-scattering formulation. *J. Phys.: Condens. Matter* **2001**, *13*, 8587−8606.
(71) Geilhufe, M.; Achilles, S.; Köbis, M. A.; Arnold, M.; Mertig, I.; Hergert, W.; Ernst, A. Numerical solution of the relativistic single-site scattering problem for the Coulomb and the Mathieu potential. *J. Phys.: Condens. Matter* **2015**, *27*, 435202.

DOI: 10.1021/acs.nanolett.7b01548
Nano Lett. 2018, 18, 1564−1574